Viser Technology Pte. Ltd.
Research and Application of Materials Science
DOI: 10.33142/rams.v5i1.11757

Research Article Open Access

Preparation of $Na_3V_2(PO_4)_3$ Cathode Materials by Hydrothermal Assisted Sol-Gel Method for Sodium -Ion Batteries

Jiayu LI

Public Experiment Center University of Shanghai for Science and Technology Shanghai 201210,P. R. China

Corresponding Author: Jiayu Li, e-mail: 249595941@qq.com

Abstract

$Na_3V_2(PO_4)_3$ (NVP) cathode material of the sodium ion battery (1 C=117 mAh g^{-1}) has a NASICON-type structure, which not only facilitates the rapid migration of sodium ions, but also has a small volume deformation during sodium ion de-intercalation and the main frame mechanism remains unchanged, and thus is seen as an energy storage material for a wide range of applications, but has a limited electronic conductivity due to its structure. In this paper, NVP cathode materials with finer primary particles are successfully prepared using a simple hydrothermal treatment-assisted sol-gel method. The increased pore size of the NVP materials prepared under the hydrothermal process allows for more active sites and more effective resistance to the volume deformation of sodium ions during insertion/extraction processes, effectively facilitating the diffusion of ions and electrons. The $Na_3V_2(PO_4)_3$ material obtained by the optimized process exhibited good crystallinity in XRD characterization, as well as superior electrochemical properties in a series of electrochemical tests. A specific capacitance of 106.3 mAh g^{-1} at 0.2 C is demonstrated, compared to 96.5 mAh g^{-1} for $Na_3V_2(PO_4)_3$ without hydrothermal treatment, and cycling performance is also improved with 93% capacity retention. The calculated sodium ion diffusion coefficient ($D_{Na} = 5.68 \times 10^{-14}$) obtained after EIS curve fitting of the improved sample illustrates that the pore structure is beneficial to the performance of the $Na_3V_2(PO_4)_3$ cathode material.

Keywords: *$Na_3V_2(PO_4)_3$; Hydrothermal assisted; Sodium ion; Porosity*

1 Introduction

The global economy exists based on the extensive use of fossil energy, the consumption of large amounts of non-renewable resources, and simultaneously brings significant environmental problems. Considering this, the most pressing strategy for mitigating the energy and environmental crisis is to proactively foster the development of new sources of energy. Addressing the issue of effective energy conversion and storage across various forms of energy has become a shared preoccupation [1-2]. As the market for large-scale energy storage and small-scale household devices continues to expand, there is an increasingly stringent demand for materials that possess ample reserves, favorable prices, and superior safety performance.

Currently, lithium-ion batteries have been further developed and become popular green secondary batteries due to advantages of high energy storage density, high specific capacity, high volumetric capacity, and long cycle life [3-4], resulting in a sharp increase in the demand for lithium. However, the continued large-scale development of limited lithium resources will inevitably lead to a significant rise in lithium material prices. It will certainly make the price of lithium materials rise significantly. In contrast, sodium has abundant reserves, low cost, and similar electrochemical properties to lithium as belong to the same main group. Sodium-ion batteries have numerous potential advantages due to the widespread distribution of resources and slightly higher voltage, which are suitable for large-scale energy storage [5-6]. Therefore, high-energy, green, environmentally friendly, and inexpensive materials for sodium-ion batteries can effectively solve problems such as lithium resource shortages and high prices. This research has important practical significance for the sustainable development of human society.

In the sodium-ion cathode material system, phosphate-based materials with open-framework

Received on March 11, 2023; Accepted on April 28, 2023

structures and thermal stability have garnered considerable attention [7]. In this case, the NASICON-type structure of $Na_3V_2(PO_4)_3$ has separate VO_6 octahedral and PO_4 tetrahedral units connected by oxygen atoms at the corners to form $[V_2(PO_4)_3]^{3-}$, each $[V_2(PO_4)_3]$ unit being connected by PO_4. The two different Na atoms are in the gaps and channels of the framework in different oxygen environments. The first station is the Na (1) site in the VO_6 octahedral vacancy in a six-coordinate environment, and the second station is the Na (2) site in the PO_4 tetrahedral vacancy in an eight-coordinate environment, with six structural units in each NVP cell, with one Na (1) site and three Na (2) sites present in each unit [8-9]. $Na_3V_2(PO_4)_3$ with a stable three-dimensional structure can enhance the reaction kinetics of sodium ions with large radii and weights during electrochemical migration and is suitable for the rapid diffusion of sodium ions, which more slight volume distortion during intercalation/deintercalation process of sodium ion. Additionally, NVP exhibits a higher storage voltage, with the charge-discharge platform situated at approximately 3.4 V. However, compared to metal oxide cathode materials, NVP displays relatively lower electrical conductivity, which has impeded its progress. Further various modifications are currently carried out by optimizing the synthesis process through controlled morphology [10-12], multiphase synthesis [13-14], and ion doping [15-16] to improve the electrochemical properties of NVP [17].

The present study synthesizes $Na_3V_2(PO_4)_3$ cathode material using a hydrothermal-assisted sol-gel method. The hydrothermal assistance aims to refine the grain size, control the morphology, and achieve continuous carbon coating, which positively influence the electrochemical performance of $Na_3V_2(PO_4)_3$ electrode material. Structure verification, morphology, and electrochemical performance of $Na_3V_2(PO_4)_3$ are characterized through a series of tests. The hydrothermally treated $Na_3V_2(PO_4)_3$ electrode material exhibits superior electrochemical performance in terms of specific capacity, rate capability, and cycling performance. The relatively lager surface porosity of H-NVP particles is conducive to fully contact the electrolyte and cathode materials, shortens the diffusion path of sodium ions, and assists the rapid transfer of sodium ions. The primary particles are finer, which helps to alleviate the volume deformation caused by the charging and discharging process and ensures the integrity of the main structure.

2 Experimental Section

2.1. Materials synthesis

Raw materials used NaOH, NH_4VO_3, $NH_3H_2PO_4$, as well as ascorbic acid as a reducing agent and carbon source. $NH_3H_2PO_4$ was dissolved in NaOH solution to obtain solution A, while NH_4VO_3 was dissolved in ascorbic acid solution to obtain solution B. Solution A was slowly added dropwise into solution B, followed by thorough mixing. The mixture was then transferred to a 40 ml stainless steel autoclave and heated at 190 ℃ for 36 hours. After cooling to room temperature, a brown solution was obtained. The solution was further heated and stirred at 75 ℃ in an air atmosphere until gel formation occurred. The gel was then dried at 60 ℃ under air ambient conditions for 12 hours, and subsequently ground into powder. Finally, the powder was segmented and calcined in a nitrogen atmosphere (4 hours at 350 ℃ and 8 hours at 800 ℃) to obtain the final product, grinding after cooling to room temperature (named H-NVP). A comparative experiment was conducted using the same experimental parameters to synthesize $Na_3V_2(PO_4)_3$ electrode material only via sol-gel (referred to as the G-NVP).

2.2. Material Characterizations and Electrochemical measurements

The crystallographic structures surface and morphology of the electrode materials were analyzed using X-ray diffraction (XRD，Rigaku, Japan) with Cu Kα radiation in the range of 10° to 60°, and scanning electron microscopy (SEM, ZEISS, SUPRA-55). The electrode consisted of three components: NVP (cathode material, 80 wt%), acetylene black (conductive agent, 10 wt%), and polytetrafluoroethylene (PVDF) (binder, 10 wt%). The $Na_3V_2(PO_4)_3$ electrode was assembled into a CR2032 coin type cell, with the electrolyte composed of ethylene carbonate (EC), dimethyl carbonate (DEC), and fluoroethylene carbonate (FEC) in 1 M NaClO4, which the volume ratio of EC to DEC is 1 to 1, and FEC is 5 wt%. A glass fiber membrane (Whatman, GF/D) as the separator, and sodium foil as the anode electrode. Charge/discharge performance, cyclic voltammetry (CV) testing (2.5-3.8 V), and electrochemical impedance spectroscopy (EIS) measurements (10^{-1} and 10^5 Hz) all at room temperature (25 ℃), using the Land2001A system, a CHI660E electrochemical workstation, and Solartron Analytical 1260A/1287A, respectively.

3. Results and Discussion

The crystal structure of the prepared electrode is detected by XRD, Figure 1a presents a comparative XRD analysis of G-NVP and H-NVP samples, showing their consistency with the JCPDS card (#00-62-0345). The diffraction peaks of the materials are relatively sharp, and the bottom of the diffraction pattern is flat, indicating that the crystallinity of the synthesized NVP is great. Both samples exhibit a R3c space group, belonging to the hexagonal crystal system. No impurity phases or carbon diffraction peaks are observed in the figure, indicating the presence of amorphous carbon and successful synthesis of pure-phase $Na_3V_2(PO_4)_3$ cathode material. H-NVP displays higher diffraction peak intensities than the G-NVP, exhibiting better crystallinity.

The SEM images of H-NVP and G-NVP show that

the morphologies of the two samples differ significantly (in Figure 1). As can be noticed from Figure 1b, H-NVP is a secondary particle formed by the agglomeration of primary particles with a size of 150 nm-250 nm. According to Figure 1c, the surface of G-NVP is relatively smooth, displaying irregular shapes, with individual small particles attached, and the size of the primary particles is around 3 μm. The primary particles of the hydrothermally treated H-NVP are obviously refined, and although agglomeration is present, the suitable number of gaps existing between the particles facilitated the transport of sodium ions. More information about morphology of the H-NVP material is obtained by TEM. It can be seen clearly from Figure 1d, H-NVP is coated with carbon and no lattice streaks associated with the surface carbon layer were observed, which proved that carbon exists in an amorphous state. The clear spacing distance with 0.289 nm correspond to the (116) plane of H-NVP in Figure 1e, indicating the successful synthesis of the H-NVP material.

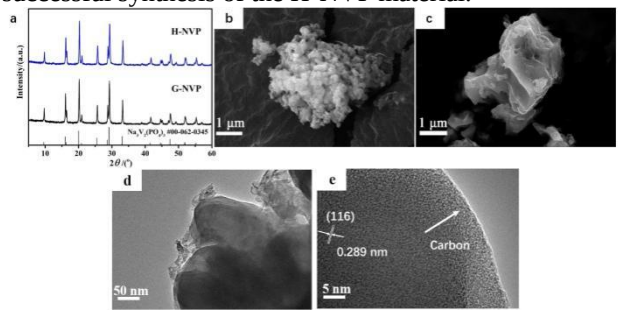

Figure 1 Structural and morphological characterization (a) XRD results for H-NVP and G-NVP; (b) SEM of H-NVP; (c) SEM of G-NVP; (d and e) TEM and HRTEM images of H-NVP.

The electrochemical properties of $Na_3V_2(PO_4)_3$/C cathode material are further characterized (Figure 2). Figure 2a shows the first charge-discharge curves of the two samples at a rate of 0.2 C and in a voltage range of 2.5-3.8 V. In fact, the $Na_3V_2(PO_4)_3$/C electrode exists two redox potentials at 3.4 V and 1.6 V, characterized by valence changes corresponding to V^{3+}/V^{4+} and V^{2+}/V^{3+}, with relative theoretical capacities of 117 mAh/g and 236 mAh/g, respectively. However, due to the instability of V^{2+} in $Na_4V_2(PO_4)_3$, the V^{3+} of $Na_3V_2(PO_4)_3$ is more favorable for the preparation of synthesis. To prevent the formation of V^{2+} during charging and discharging, the charging and discharging voltages are usually limited to control the electrochemical reactions, resulting in a reversible conversion of vanadium [18]. The working plateau at 3.4 V corresponds to the transition between $Na_3V_2(PO_4)_3$ and $NaV_2(PO_4)_3$ phases. The charge-discharge plateaus of the G-NVP (3.4242/3.3367 V) are widely separated (potential difference ΔV=87.5 mV), indicating severe polarization, while those of the H-NVP (3.3984/3.3473 V, ΔV=51.1 mV) are flatter and more prolonged, indicating good reversibility of the material. The initial discharge specific capacities of G-NVP and H-NVP are 96.5 mAh g^{-1} and 106.3 mAh g^{-1}, respectively. The reduced polarization and stable operating voltage plateau during the electrochemical process allows H-NVP to have a higher specific capacitance.

The cycling performance of G-NVP and H-NVP is shown in Figure 2b. Both samples are cycled between 2.5 and 3.8 V at a rate of 0.2 C, the H-NVP provided a discharge specific capacity of 98.86 mAh g^{-1} after 500 cycles, which a loss of only 7% compared to the initial discharge capacity. In contrast, the specific capacity of G-NVP decreases by 20% under the same conditions. The H-NVP undergoing hydrothermal treatment exhibits better capacity retention and cycling stability, which is shown that this means can improve the electrochemical performance of $Na_3V_2(PO_4)_3$/C cathode material, and the enhancement of cycling stability is related to the effective alleviation of the volume effect of the electrode material during charging and discharging, keeping the structure stable [19].

Likewise, the rate properties of all samples are examined in half-cells to determine capacity retention in response to changes in current density. The rate capabilities of H-NVP and G-NVP are shown under different current densities of 0.2, 0.5, 1, 2, 5, 10, and 20 C in Figure 2c. Obviously, the discharge capacity decreases with increasing current density. In the voltage range of 2.5-3.8 V, H-NVP shows better rate capability and has a smaller capacity difference between 0.2 C and 20 C. The discharge capacities of H-NVP at 0.2, 0.5, 1, 2, 5, 10, and 20 C are 105.8, 101.6, 95.9, 94.5, 85.3, 79.9 and 76.2 mAh g^{-1} respectively. It is of interest that the difference specific capacities of H-NVP and G-NVP are more stable at small current densities (0.2, 0.5 ,1, 2 C). As the current density intensifies, the difference is larger at higher current densities (5, 10, 20 C). The G-NVP capacity decays more significantly at 20 C to 62.3 mAh g^{-1}, and when the current density returned to 0.2 C, the H-NVP capacity remains at approximately 104.3 mAh g^{-1}, maintaining 98.6 % of the initial capacity. Even under high rates of 20 C, the discharge specific capacity still exceeds 75 mAh g^{-1}, mainly due to more pores, which allows for more complete contact between the cathode material and electrolyte, increases the active sites of the reaction process, provide more sodium ion migration channels，and facilitates the diffusion of sodium ions. More sodium ion migration channels are provided, so that H-NVP can maintain a high specific capacitance even in the process of high-rate rapid charge and discharge.

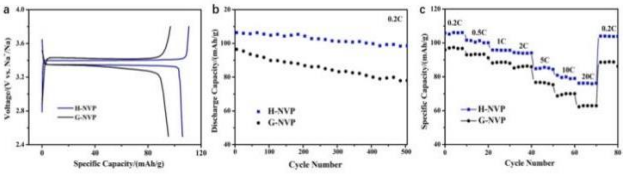

Figure 2 Electrochemical testing for H-NVP and G-NVP (a) The first charge and discharge curve at 0.2 C; (b) Cycle at 0.2 C (c) Rate at 0.2, 0.5, 1, 2, 5, 10, and 20 C

To better investigate the electrode reaction kinetics, cyclic voltammetry (CV) is used to analyze the NVP electrode material. The cyclic voltammetry curves of G-NVP and H-NVP at a scan rate of 0.1 mV/s, which corresponds to the first charge/discharge plateau (3.4 V) in Figure 3a. The peaks at 3.448 V and 3.289 V (vs. Na^+/Na) of H-NVP represent the Na^+ insertion (oxidation)/extraction (reduction) processes, which are attributed to the oxidation-reduction of V^{4+}/V^{3+} in $Na_3V_2(PO_4)_3/C$, resulting in the transformation between $Na_3V_2(PO_4)_3$ and $NaV_2(PO_4)_3$ phases, as shown in reaction equation (1) [20]. H-NVP exhibits high current intensity, sharp peaks, and symmetrical peak areas, demonstrating an improved diffusion rate of Na^+ of H-NVP [21]. The potential difference (ΔV) of the oxidation-reduction peaks is inversely proportional to the degree of reversible phase transition during the electrochemical reaction of the cathode material. A larger value of ΔV indicates more severe polarization of the material. Compared to G-NVP (ΔV=0.24 V), H-NVP has a potential difference of approximately 0.159 V, likewise making known a lower polarization effect.

$$Na_3V_2^{3+}(PO_4)_3 \Leftrightarrow NaV_2^{4+}(PO_4)_3 + 2Na^+ + 2e^- \quad (1)$$

The stability of the electrochemical properties of H-NVP is further explored by CV, before charging and discharging the H-NVP sample for the first 3 cycles as shown in Figure 3b. The oxidation/reduction peak positions of H-NVP remained almost unchanged during the three cycles, indicating the high stability and reversibility of Na^+ in the de intercalate process [22]. Observation of the CV curves reveals that the current intensity of the second loop is slightly lower than that of the first loop, which may be caused by a small amount of irreversible phase change [23], and the subsequent third loop curves almost completely overlap in both peak position and peak intensity, and the results imply the good structural stability and reversibility of the reaction of the material，which is consistent with the above electrochemical test results

To further study the electrochemical process of NVP cathode material, electrochemical impedance spectroscopy (EIS) is performed prior to charging and discharging in the frequency range of 10^{-1} Hz to 10^5 Hz. Figure 3c shows the Nyquist plots and fitted equivalent circuits for both sets of samples. The EIS plots consist of two parts: the high-frequency range semicircle attributed to charge transfer resistance (R_{ct}) [24], and the sloping line in the low-frequency region corresponding to Warburg impedance (Z_w), related to the diffusion of Na^+. In the high frequency range, the Z-axis intercept corresponds to the complex resistance (R_e) of the electrolyte and electrode, which is approximately 7 Ω for all electrodes. the CPE is related to the surface properties [25-26]. By fitting, the charge transfer resistances of H-NVP and G-NVP are determined to be 294.94 Ω and 477.75 Ω, respectively. This is attributable to the smooth particle surface and oversized of G-NVP particles, hindering sufficient contact between the electrolyte and the cathode material, which is not conducive to the transfer of electrons and decreases the conductivity. It is suggested that the addition of the hydrothermal processing step leads to an increase in the electronic conductivity. The diffusion coefficient (D_{Na}) of sodium ions can be estimated from the low frequency region using the following equation (2) [27]:

$$DNa = \frac{0.5R^2T^2}{S^2n^4F^4C^2\sigma^2} \quad (2)$$

R is the gas constant, T is the absolute temperature, S is the effective surface area of the cathode, n is the number of electrons per substance reacted in the oxidation process, F is the Faraday constant, C is the concentration of Na ions (related to the chemical composition of the given active substance, about 6.92 × 10^{-3} mol cm^{-3}), and σ is the Warburg factor associated with Z':

$$Z' = Re + Rct + \sigma\omega^{-1/2} \quad (3)$$

Figure 3d shows the linear fit of Z' and ω, whose slope can be used to calculate the diffusion coefficient of sodium ions. According to Eq. (3), σ is obtained as 36.73, 106.02 for the H-NVP and G-NVP samples, respectively, and the corresponding D_{Na} is calculated to be equal to 5.68 × 10^{-14}, 6.67 × 10^{-15}, respectively, when substituted into Eq. (2). H-NVP exhibits a larger sodium ion diffusion coefficient, which is due to the pore structure between the refined grains that facilitates the of sodium ions and shortens the diffusion distance of sodium ions.

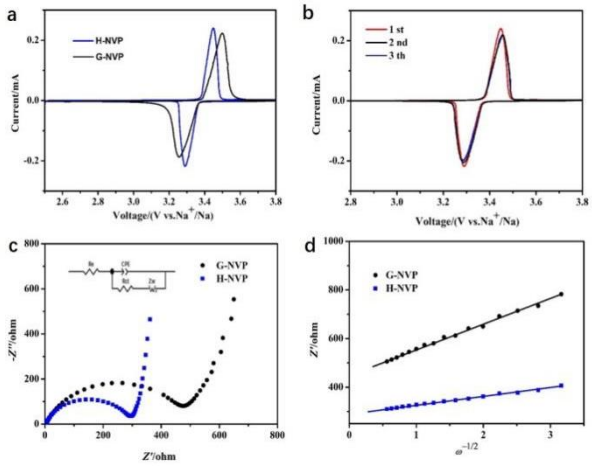

Figure 3 Electrochemical performances for H-NVP and G-NVP (a) CV curves; (b) three CV curves without charging and discharging for H-NVP; (c) EIS Spectrum; (d) Plot of Z' vs $\omega^{-1/2}$.

4. Conclusion

In this study, the synthesis process of $Na_3V_2(PO_4)_3/C$ is optimized. With the addition of a

hydrothermal treatment process, more refined primary particles are obtained, and the presence of significant pores in the secondary particles facilitated the electron and ion transport between the active particles. A series of electrochemical tests verified the improved performance of the H-NVP cathode material. The presence of pores allowed a more adequate contact between the cathode material and the electrolyte, and the active sites of the material increased, allowing a capacity of 75 mAh g^{-1} to be achieved even at high magnification (20 C). CV curves of H-NVP (ΔV=0.159 V) compared to G-NVP with ΔV=0.24 V, and three curves CV of H-NVP (under uncharged and discharged tests) are highly overlapping, indicating that H-NVP possesses better reversibility and the transfer of electrons and ions between active particles is greatly improved.

References

[1] Sun B X, Zhao X Z, et al., Virtual Battery Pack-Based Battery Management System Testing Framework, Energies, 2023, 16, 680, https://doi.org/10.3390/en16020680

[2] Singh A N, Nam K W, Solid-state synthesized batteries get upset, Matter, 2022, 5, 1347–1349, https://doi.org/10.1016/j.matt.2022.04.003

[3] Li M, Lu J, Chen Z, et al., 30 Years of Lithium-Ion Batteries, Advanced Materials, 2018, 30, 1800561, https://doi.org/10.1002/adma.201800561.

[4] Chen S, Wu C, Shen L, et al., Challenges and perspectives for NASICON-Type electrode materials for advanced sodium-ion batteries, Advanced Materials, 2017, 29, 1700431, https://doi.org/10.1002/adma.201700431.

[5] Zhang W L, Yin J, et al., Status of rechargeable potassium batteries, Nano Energy, 2021, 83, 105792, https://doi.org/10.1016/j.nanoen.2021.105792.

[6] Ren W, Zhu Z, An Q, et al., Emerging prototype sodium-ion full cells with nanostructured electrode materials, Small, 2017, 13, 1604181, https://doi.org/10.1002/smll.201604181.

[7] Yabuuchi N, Kubota K, et al., Research development on sodium-ion batteries, Chemical Reviews, 2014, 114, 11636-11682, https://doi.org/10.1021/cr500192f.

[8] Jian Z, Zhao L, Pan H, et al., Carbon coated $Na_3V_2(PO_4)_3$, as novel electrode material for sodium ion batteries, Electrochemistry Communications, 2012, 14, 86-89, https://doi.org/10.1016/j.elecom.2011.11.009.

[9] Park S, Wang Z L, et al., Crystal Structure of $Na_2V_2(PO_4)_3$, an Intriguing Phase Spotted in the $Na_3V_2(PO_4)_3$–$Na_1V_2(PO_4)_3$ System, Chemistry of Materials, 2022, 34, 451-462, https://doi.org/10.1021/acs.chemmater.1c04033.

[10] Chen H, Huang Y, Mao G, et al., Reduced graphene oxide decorated $Na_3V_2(PO_4)_3$ microspheres as cathode material with advanced sodium storage performance, Frontiers in Chemistry, 2018, 6, 174, https://doi.org/10.3389/fchem.2018.00174.

[11] Jiang Y, Zhou X, Li D, et al., Highly Reversible Na Storage in $Na_3V_2(PO_4)_3$ by Optimizing Nanostructure and Rational Surface Engineering, Advanced Energy Materials, 2018, 8, 1800068, https://doi.org/10.1002/aenm.201800068.

[12] Bao S, Huang Y Y, et al., Porous $Na_3V_2(PO_4)_3$ as cathode material for high-rate sodium-ion batteries by sacrificed template method, Ionics, 2020, 26, 5011–5018, https://doi.org/10.1007/s11581-020-03635-0.

[13] Wang C, Long H, et al., A multiphase sodium vanadium phosphate cathode material for high-rate sodium-ion batteries, Journal of Materials Science & Technology, 2021, 66, 121–127, https://doi.org/10.1016/j.jmst.2020.05.076.

[14] Senthilkumar B, Murugesan C, et al., Electrochemical insertion of potassium ions in $Na_4Fe_3(PO_4)_2P_2O_7$ mixed phosphate, Journal of Power Sources, 2020, 480, 228794, https://doi.org/10.1016/j.jpowsour.2020.228794.

[15] Tian Z Y, Chen Y J, et al., Boosting the rate capability and working lifespan of K/Co co-doped $Na_3V_2(PO_4)_3$/C for sodium ion batteries, Ceramics International, 2021, 47, 22025-22034, https://doi.org/10.1016/j.ceramint.2021.04.222.

[16] Jiang X M, Liu C C, et al., Constructing p-type substitution induced by Ca^{2+} in defective $Na_3V_{2-x}Ca_x(PO_4)_3$/C wrapped with conductive CNTs for high-performance sodium-ion batteries, Dalton Transactions, 2022, 51, 16145–16157, https://doi.org/ 10.1039/d2dt02602c.

[17] Li J H, Chen Y J, et al., Mechanisms and principles of $Na_3V_2(PO_4)_3$ modification by carbon materials, Current Opinion in Electrochemistry, 2023, 37, 101200, https://doi.org/10.1016/j.coelec.2022.101200.

[18] Lim S Y, Kim H, Shakoor R A, et al., Electrochemical and Thermal Properties of NASICON Structured $Na_3V_2(PO_4)_3$ as a Sodium Rechargeable Battery Cathode: A Combined Experimental and Theoretical Study, Journal of the Electrochemical Society, 2012, 159, A1393-A1397, DOI 10.1149/2.015209jes.

[19] Cheng J, Chen Y J, et al., $Na_3V_2(PO_4)_3$/C·$Na_3V_2(PO_4)_2F_3$/C@rGO blended cathode material with elevated energy density for sodium ion batteries, Ceramics International, 2021, 47, 18065–18074, https://doi.org/10.1016/j.ceramint.2021.03.122.

[20] Duan W, Zhu Z, Li H, et al., $Na_3V_2(PO_4)_3$@C core-shell nanocomposites for rechargeable sodium-ion batteries, Journal of Materials Chemistry A, 2014, 2, 8668-8675, DOI: 10.1039/c4ta00106k.

[21] Jiang Y, Yang Z Z, et al., Nanoconfined Carbon-Coated $Na_3V_2(PO_4)_3$ Particles in Mesoporous Carbon Enabling Ultralong Cycle Life for Sodium-Ion Batteries, Advanced Energy Materials, 2015, 5, 1402104, https://doi.org/10.1002/aenm.201402104 .

[22] Delmas C, Braconnier J J, Fouassier C, et al., Electrochemical intercalation of sodium in Na_xCoO_2

bronzes, Solid State Ionics, 1981, 3, 165-169, https://doi.org/10.1016/0167-2738(81)90076-X.

[23] Keller M, Buchholz D, Passerini S. Layered Na-Ion Cathodes with Outstanding Performance Resulting from the Synergetic Effect of Mixed P- and O-Type Phases, Advanced Energy Materials, 2016, 6, 1501555-1501565, https://doi.org/10.1002/aenm.201501555.

[24] Li G R, Song J, Pan G L, et al., Highly Pt-like electrocatalytic activity of transition metal nitrides for dye-sensitized solar cells, Energy & Environmental Science, 2011, 4, 1680-1683, https://doi.org/10.1039/C1EE01105G.

[25] Du K, Guo H, Hu G, et al.. Na3V2(PO4)3 as cathode material for hybrid lithium ion batteries, Journal of Power Sources, 2013, 223, 284-288, http://dx.doi.org/10.1016/j.jpowsour.2012.09.069.

[26] Li G, Jiang D, Wang H, et al.. Glucose-assisted synthesis of Na3V2(PO4)3/C composite as an electrode material for high-performance sodium-ion batteries, Journal of Power Sources, 2014, 265, 325-334, http://dx.doi.org/10.1016/j.jpowsour.2014.04.054.

[27] Su R Y, Zhu W K, et al.. Mnx+ Substitution to Improve Na3V2(PO4)2F3-Based Electrodes for Sodium-Ion Battery Cathode, Molecules, 2023, 28, 1409, https://doi.org/10.3390/molecules28031409.